Diagenetic pathways linked to labile Mg-clays in lacustrine carbonate reservoirs: a model for the origin of secondary porosity in the Cretaceous pre-salt Barra Velha Formation, offshore Brazil

NICHOLAS J. TOSCA[1,2]* & V. PAUL WRIGHT[3]

[1]*Department of Earth & Environmental Sciences, University of St Andrews, St Andrews KY16 9AL, UK*

[2]*Present address: Department of Earth Sciences, University of Oxford, Oxford OX1 3AN, UK*

[3]*PW Carbonate Geoscience Ltd and Natural Sciences (Geology), National Museum of Wales, Cathays Park, Cardiff CF10 3NP, UK*

**Correspondence: nickt@earth.ox.ac.uk*

Abstract: The lacustrine carbonate reservoirs of the South Atlantic host significant accumulations of chemically reactive and Al-free Mg-silicate minerals (e.g. stevensite, kerolite and talc). Petrographic data from units such as the Cretaceous Barra Velha Formation in the Santos Basin suggest that Mg-silicate minerals strongly influenced, and perhaps created, much of the observed secondary porosity. The diagenetic interactions between reactive Mg-silicate minerals and carbonate sediments are, however, poorly known. Here we develop a conceptual model for the origin of secondary porosity in the Barra Velha Formation guided by considerations of the chemistry that triggers Mg-silicate crystallization, as well as the geochemical and mineralogical factors that act as prerequisites for rapid Mg-silicate dissolution during early and late diagenesis. We conclude that sub-littoral zones of volcanically influenced rift lakes would have acted as the locus for widespread Mg-silicate accumulation and preservation. Organic-rich profundal sediments, however, would be especially prone to Mg-silicate dissolution and secondary porosity development. Here, organic matter diagenesis (especially methanogenesis) plays a major role in modifying the dissolved inorganic carbon budget and the pH of sediment porewaters, which preferentially destabilizes and then dissolves Mg-silicates. Together, the sedimentological, stratigraphic and geochemical predictions of the model explain many enigmatic features of the Barra Velha Formation, providing a novel framework for understanding how Mg-silicate–carbonate interactions might generate secondary porosity more broadly in other lacustrine carbonate reservoirs across the South Atlantic.

The proposal that carbonate-hosted porosity in the large oil fields in the Barra Velha Formation of the Santos Basin, offshore Brazil, is a result of the dissolution of Mg-silicates, such as stevensite (Wright & Barnett 2015), raises the possibility that an unstudied diagenetic system strongly influences the properties of lacustrine carbonates. To address this issue, this paper reviews the distribution and diagenetic behaviour of Mg-silicates, especially those associated with rift basins such as those currently the focus of intense exploration in the South Atlantic. Based on these considerations, we develop a model for understanding how Mg-silicate–carbonate interactions lead to the generation of secondary porosity in lacustrine reservoirs such as the Barra Velha Formation.

Lake systems developed on rifted margins, specifically those that are volcanically influenced, produce a wide variety of carbonate sediments (Renaut *et al.* 2002; Gierlowski-Kordesch 2010; Wright 2012). In these settings, the lithology of the surrounding catchment influences lake-water chemistry, which, in turn, controls the style of carbonate production (Jones & Bowser 1978; Wright 2012). Lakes developed on volcanic catchments tend to feature waters rich in Ca, Mg, $SiO_{2(aq)}$ and HCO_3^-, commonly reaching alkaline pH values (Yuretich & Cerling 1983; Cerling 1994). This chemistry commonly triggers the formation of Mg-rich clay minerals (here collectively referred to as Mg-silicates) that are abundant products of alkaline lake systems. Nevertheless, despite their frequent occurrences in these systems, Mg-silicates have received little attention from the standpoint of carbonate reservoir properties.

Mg-silicates are the most geochemically reactive of all of the clay mineral groups; they form very early during peri-marine and lacustrine sediment

From: Armitage, P. J., Butcher, A. R., Churchill, J. M., Csoma, A. E., Hollis, C., Lander, R. H., Omma, J. E. & Worden, R. H. (eds) 2018. *Reservoir Quality of Clastic and Carbonate Rocks: Analysis, Modelling and Prediction*. Geological Society, London, Special Publications, **435**, 33–46.
First published online November 20, 2015, https://doi.org/10.1144/SP435.1

diagenesis, and are known to precipitate directly (and very rapidly) from the water column, setting them apart from other clay minerals (Millot 1970; Jones 1986). Because they exhibit marked variation in response to changes in pH, cation chemistry, salinity and the presence/absence of Al-bearing detrital material, Mg-rich clays have long been recognized as valuable tools in developing facies models for lacustrine environments. Most notably, Millot (1970) developed a facies model for the distribution of Mg-rich clays in closed-basin settings that has largely withstood the test of time. The model places the most Al- and Fe-rich clay minerals at the basin margins, as aluminosilicate detritus becomes more important, with clay mineral chemistry progressively becoming more Mg- and Si-rich (and Al-poor) towards the basin centre. Eventually, clays formed in the centre of the basin are dominated by Mg-rich smectite (i.e. stevensite), kerolite and sepiolite. This model, and the decades of subsequent work refining it (see more expanded discussions in Jones 1986; Calvo *et al.* 1999; Deocampo *et al.* 2009; Tosca 2015), places lacustrine clay mineral formation and Mg-silicates within an easily understood depositional framework. Nevertheless, predicting the distribution of Mg-rich clays on a thermodynamic basis has been hindered by gaps in the understanding of the Mg-silicate crystallization process (Jones 1986; Galán & Pozo 2011; Tosca 2015).

Although the formation of lacustrine Mg-silicates has received considerable attention, the diagenesis of Mg-silicate clay minerals and the processes that drive dissolution and generate porosity in lacustrine carbonates have received very little. In the following sections, we explore this process from a number of perspectives. We start by introducing the major structural characteristics of the most common lacustrine Mg-rich clay minerals and examine the processes that lead to their formation. This background makes it easier to understand why Mg-silicates are so susceptible to destruction during early and later diagenesis of lacustrine carbonates, as we discuss below.

Structural factors influencing Mg-silicate formation and diagenesis

Although there are a number of Mg-rich silicate phases that are known to occur in lacustrine carbonates (Pozo & Casas 1999; Galán & Pozo 2011; Bristow *et al.* 2012), they all share many structural characteristics and have nearly identical chemical compositions. The most common Mg-silicates deposited with lacustrine carbonates are composed almost exclusively of Mg and Si, with only stevensite containing additional cations, most commonly Na. As a consequence, the crystal structures of these phases are closely related but differ significantly in detail (Brindley *et al.* 1977; Bailey 1980; Guggenheim & Eggleton 1987; Guggenheim & Krekeler 2011). This overall structural similarity offers a possible explanation for the common co-occurrence and broadly similar geochemical affinity of Mg-silicates for saline alkaline environments. However, the subtle structural details that distinguish one phase from another mean that each Mg-silicate has specific genetic significance that lends detailed insight into the sedimentary and geochemical environment of deposition.

The lacustrine Mg-silicates are all built loosely on permutations of the talc structure. The crystal structure of talc is composed of a 'TOT' (also referred to as a 2:1 type) structure, whereby layers of Mg-octahedra ('O' layers) are effectively sandwiched by two layers of Si-tetrahedra ('T' layers), attached at the top and bottom of the octahedral layer (Fig. 1). Because talc contains an octahedral sheet composed only of Mg with no substitution in the tetrahedral or octahedral layer, the layers have no permanent charge and therefore no expandability or interlayer cations can be accommodated (Bailey 1980; Evans & Guggenheim 1988; Drits *et al.* 2012). Kerolite, a common lacustrine Mg-silicate, is most intuitively viewed as a hydrated variety of the talc structure. Here, interlayer and surface adsorbed H_2O lead to a slightly larger interlayer repeat distance (Fig. 1), although the details of how this is accommodated are not well known (Brindley *et al.* 1977; Miller *et al.* 1991). Because of these close similarities, kerolite in practice is commonly mistaken for talc (and vice versa). However, in most sedimentary environments that give rise to Mg-silicates, kerolite precipitates initially and talc (*sensu stricto*) formation usually results from prolonged dehydration: for example, upon burial diagenesis (Mitsuda & Taguchi 1977; Noack *et al.* 1989; Tosca *et al.* 2011). Stevensite, yet another common lacustrine Mg-silicate, is broadly similar to talc and kerolite, except that the Mg-octahedral layer contains a number of cation vacancies that impart a low but permanent negative charge to the structure: this must be accommodated by positively charged interlayer cations (Fig. 1) (Faust & Murata 1953; Faust *et al.* 1959; Wilson 2013). This classifies stevensite as an expandable clay and member of the smectite group, but overall its structure still shares many structural similarities with talc and kerolite. Finally, sepiolite is composed of 'TOT ribbons' of Mg-octahedra and Si-tetrahedra (Guggenheim & Krekeler 2011). These ribbons run parallel with the crystallographic *x*-axis and, when linked together at their corners, form voids or channels that accommodate molecular H_2O (Fig. 1).

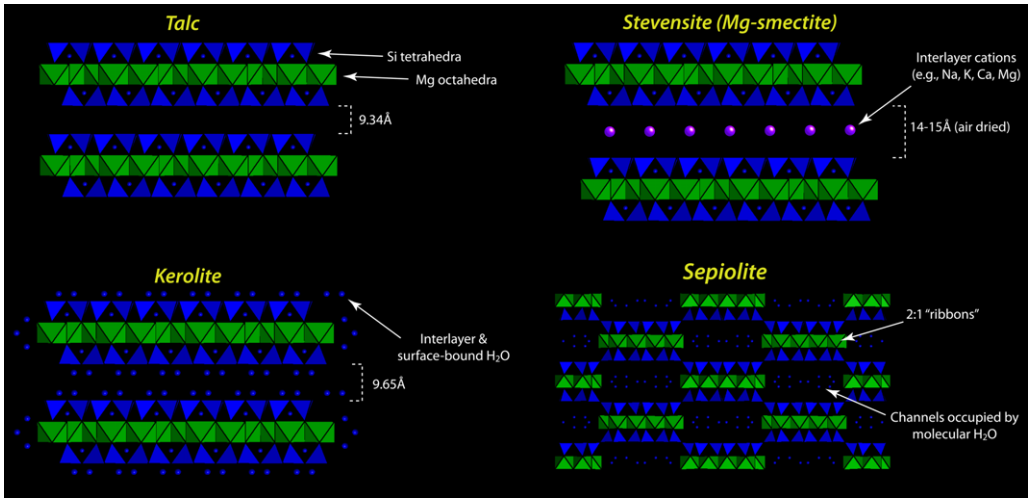

Fig. 1. A comparison of major structural features of common lacustrine Mg-silicate minerals, showing that all of the minerals under consideration are built from permutations of a 2:1 arrangement of Si tetrahedra and Mg octahedra, and are nominally free of Al.

From the standpoint of reservoir quality, the lacustrine Mg-silicate minerals discussed above share one critical feature that sets them apart from the rest of the clay mineral family: they do not contain appreciable levels of Al^{3+}. The lack of Al^{3+} allows these phases to be precipitated with relative ease directly from most natural waters (because Al^{3+} is normally insoluble under the chemical conditions of most surface waters). Also, the absence of Al^{3+} has direct consequences for Mg-silicate dissolution rates and mechanisms, which in turn places strict limits on the range of secondary products that might be formed upon their destruction.

Without Al^{3+}, the structures of the lacustrine Mg-silicates are composed entirely of Mg–O and Si–O bonds, and this strongly influences their dissolution kinetics compared to Al-bearing counterparts (Oelkers 2001*a*, *b*; Saldi *et al.* 2007). The dissolution of silicate minerals typically proceeds through the breaking of metal–oxygen bonds, which can occur at different rates depending on the bond types present (Oelkers 2001*a*, *b*). Thus, as a silicate mineral dissolves, metals are extracted from the structure in the relative order of their bond disruption rates. Of course, to maintain charge balance within the structure, proton (H^+) exchange necessarily accompanies metal release, causing H–O bonds to be formed to replace broken metal–O bonds (Oelkers 2001*a*, *b*).

One consequence of the structures discussed above is that Mg–O bonds are destroyed faster than both Al–O and Fe(III)–O bonds, both of which tend to be common in other aluminosilicates such as illite or montmorillonite (Casey & Westrich 1992; Oelkers 2001*a*, *b*). Mg–O bonds are also destroyed faster than Si–O bonds. There is abundant evidence to support these trends, including the more rapid release of Mg from serpentine, forsterite and enstatite (Casey & Ludwig 1995; Oelkers 2001*a*, *b*; Oelkers & Schott 2001), as well as antigorite, talc and phlogopite dissolution (Saldi *et al.* 2007; Brantley 2008). In drawing analogies with silicate mineral dissolution and ligand exchange reactions that occur around a particular cation, Casey & Ludwig (1995) noted that bond destruction rates strongly correlate with H_2O exchange rates around a given cation (which also correlate with bond strength). Indeed, H_2O exchange rates for Mg^{2+} are orders of magnitude faster than for Al^{3+} and Fe^{3+}, providing a mechanistic basis for observed differences in dissolution rates among silicates.

Given the variation in metal–O bond disruption rates, it follows that the slowest metal–oxygen bond to break that holds the mineral structure together therefore becomes rate-limiting (Oelkers 2001*a*, *b*; Saldi *et al.* 2007). The overall mineral dissolution rate is then a function of whether this bond disruption rate is accelerated or decelerated under specific conditions. Importantly, however, not all bonds need to be broken to completely destroy a mineral structure. For example, in the Mg-olivine mineral forsterite, Mg–O bonds are the rate-limiting step simply because their destruction liberates silica tetrahedra without needing to break Si–O bonds (because the SiO_4 tetrahedra are isolated from one another: Oelkers 1999, 2001*a*, *b*).

Mg-rich clay minerals appear to dissolve in a similar fashion, with a mechanism dictated by the specifics of the crystal structures discussed above. For example, under acidic conditions, the rates of proton exchange for Mg^{2+} in the octahedral sheet are so rapid that as this proceeds inwards from the edges, partially detached silica species are liberated in the process, in turn leading to increased surface area and further accelerated rates of dissolution (Saldi *et al.* 2007).

Together, the distinctly Al-free composition and similar structures of the Mg-rich silicates leads to dissolution rates that are much more rapid than the other aluminosilicate minerals. Most importantly, Al-free compositions lead to congruent dissolution insofar as all mineral components are liberated into solution without the formation of secondary aluminosilicates. This makes specific predictions for the range of possible products produced once Mg-silicates dissolve. However, predicting the occurrence of secondary porosity resulting from Mg-rich clay dissolution logically involves understanding the processes responsible for their original distribution within lacustrine facies.

Chemical controls on Mg-silicate formation in lacustrine sediments

A brief inspection of the chemical formulas of the Al-free Mg-silicates indicates that their stabilities will be affected by dissolved Mg^{2+}, $SiO_{2(aq)}$, pH and salinity. Indeed, natural occurrences of Al-free Mg-silicates in saline alkaline lake settings, combined with laboratory synthesis studies, indicate that these variables are responsible for the formation of one particular phase over another in most environments (Jones 1986; Jones & Galan 1988; Galán & Pozo 2011; Jones & Conko 2011). However, although the most important chemical variables in driving Mg-rich clay formation have long been recognized, predicting the occurrence of Mg-silicates from natural waters has historically been difficult and difficulties are often attributed sluggish precipitation kinetics.

The chemical and physical processes that lead to Mg-rich clay formation are easier to understand if placed within the broader context of mineral nucleation and crystal growth kinetics. Like most other minerals, clay precipitation first involves nucleation (the *de novo* generation of crystal nuclei) and then crystal growth. Mg-silicates may nucleate directly from water (termed homogeneous nucleation) or on the surface of a pre-existing solid (termed heterogeneous nucleation: Stumm 1992; Tosca 2015). Classical nucleation theory states that the homogeneous nucleation of Mg-silicates from water necessarily requires a critical level of supersaturation to be overcome (Stumm 1992). This critical supersaturation boundary predicts that spontaneous nucleation will not occur unless a given water is many times more supersaturated than equilibrium solubility predicts.

Until recently, the critical supersaturation boundary that triggers Mg-silicate nucleation from water was not well known, but a recent review of experimental synthesis data (Tosca 2015) delineated a clear boundary in more quantitative terms. This boundary can be expressed in terms of a 'Mg-silicate solubility diagram' that captures the three major chemical controls on Mg-silicate formation (i.e. $a_{SiO_2(aq)}$, $a_{Mg^{2+}}$ and pH, or a_{H^+}) (Jones 1986; Jones & Galan 1988) (Fig. 2). Figure 2 shows that this nucleation boundary lies well above the equilibrium solubilities for Mg-silicate minerals, implying that significant supersaturation is required to initiate nucleation. Figure 2 also shows that a number of different combinations of pH, Mg^{2+} and $SiO_{2(aq)}$ may result in the formation of Mg-silicates directly from water, but the individual phase that grows from such nuclei (e.g. stevensite, kerolite or sepiolite) is dependent on the kinetics of subsequent crystal growth (Jones 1986; Tosca & Masterson 2014; Tosca 2015).

Most importantly, the nucleation boundary in Figure 2 indicates why the evaporative concentration of some lake waters leads to the formation of Mg-silicates from solution and some do not. Unless this boundary is crossed, Mg-silicates will not precipitate directly from water, regardless of the phase. As Figure 2 shows, at higher $SiO_{2(aq)}$ concentrations (or activities), lower Mg and/or pH is required to overcome the nucleation boundary. This boundary also provides further support for why the most common formation pathway for stevensite is now widely recognized as authigenic precipitation from lake water (Wilson 2013). Critically, any process that results in a rapid or sudden supersaturation above this boundary will result in Mg-silicate precipitation directly from water. Such a process could include porewater modification by biological activity, mixing of water sources (e.g. hot spring input) or, much more commonly, evaporative concentration. The type of Mg-silicate formed is sensitive to the pH, Mg/Si ratio, salinity, $SiO_{2(aq)}$ input and temperature under which crystal growth occurs.

The nucleation boundary discussed above also agrees with geochemical and mineralogical analyses of evaporating saline lakes. Combined mineralogical and lake-water analyses reported in Gac *et al.* (1977) and Darragi & Tardy (1987) offers a clear example. These authors showed that in Lake Yoa of Northern Chad, authigenic stevensite precipitates with aragonite. Although aragonite is commonly formed from the Lake Yoa waters, the authigenic carbonate phase associated with

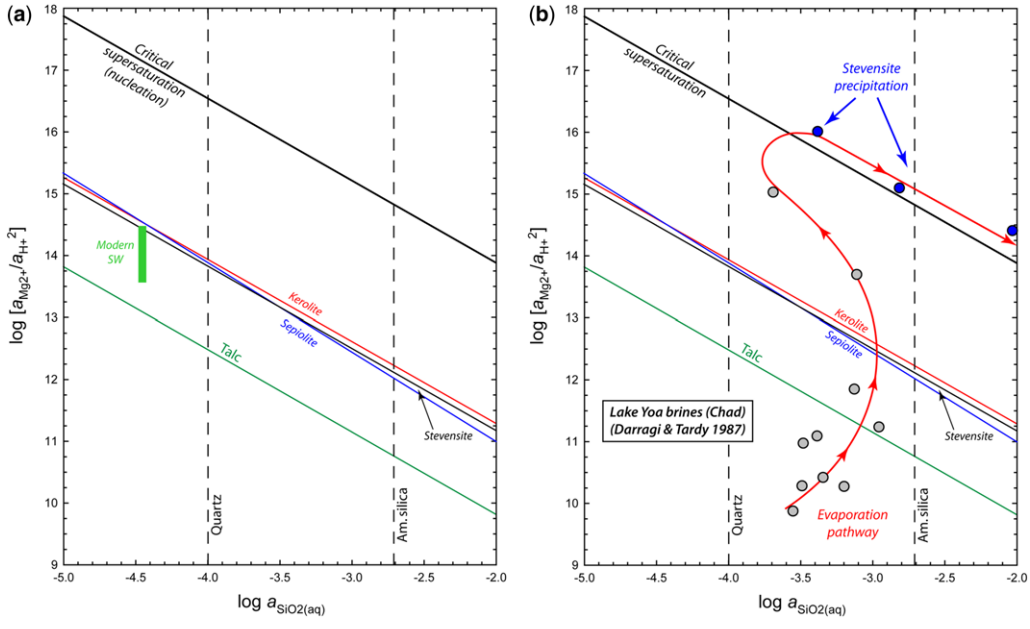

Fig. 2. **(a)** Solubility diagram for the $Mg–SiO_2–H_2O$ system at 25°C. The diagram illustrates the solubility of Mg-silicates for water compositions that have increasing Mg^{2+} concentrations and/or pH (larger *y*-axis values) or increasing $SiO_{2(aq)}$ concentrations (larger *x*-values). Water compositions plotting on or above a given boundary indicate supersaturation with respect to the Mg-silicate phase of interest. Note that the 'critical supersaturation' boundary delineated by experimental studies (Tosca 2015) corresponds to the point at which nucleation of Mg-silicates will occur directly from water with no available substrate. Modern seawater (SW) is plotted for reference, and shows why nucleation of Mg-silicates does not occur. Vertical dashed lines indicate solubilities for quartz and amorphous silica. **(b)** Chemical evolution of waters from Lake Yoa indicating the effects of evaporative concentration (data from Darragi & Tardy 1987). Waters from which stevensite has precipitated are plotted as blue circles. Sources of thermodynamic data are detailed in Tosca (2015).

Mg-silicate mineralization may vary even within the Lake Chad system, illustrating the varying impact of Mg-silicates on the resulting Ca/Mg ratio of solution (e.g. Gac *et al.* 1977; Eugster & Jones 1979; Darragi & Tardy 1987). For example, authigenic low-Mg calcite has been observed to crystallize with Mg-silicates in the Pantanal wetlands of Brazil (Barbiéro *et al.* 2002), and, indeed, Mg-silicates and low-Mg calcitic spherules both crystallized early in the history of the Barra Velha precursor sediment (Wright & Barnett 2015). Regardless of the identify of the main carbonate phase, however, the chemical evolution of the evaporating water in Lake Yoa follows a pathway illustrated in Figure 2. This pathway agrees with the supersaturation levels predicted from synthesis studies, and represents an important step in understanding when and where Mg-silicates are likely to form. This also provides some of the most convincing evidence that the main genetic pathway for widespread stevensite formation is through evaporative concentration.

The relationships discussed above can be used to make predictions regarding the distribution of Mg-silicates in lacustrine systems. Clearly, homogeneous nucleation of Mg-silicates directly from water is one of the only mechanisms that will result in the most laterally extensive accumulations of Mg-silicates. This is simply because climatic controls (e.g. evaporative hydrological regimes) act over regionally extensive areas. In contrast, the nucleation of Mg-silicates on pre-existing surfaces (e.g. heterogeneous nucleation, which requires lower levels of supersaturation) is critically dependent on the nature and distribution of the substrate itself (Tosca 2015). A number of substrates may act as favourable surfaces that cause Mg-silicate nucleation (e.g. amorphous silica, detrital certain clay minerals and biological materials, such as extracellular polymeric substances (EPS)), but this process is arguably most important when favourable chemistry and favourable surface properties (e.g. binding properties that decrease Mg-silicate–solution interfacial energy: Tosca 2015) coincide in more locally confined environments, such as microbial mats (Leveille *et al.* 2002; Souza-Egipsy *et al.* 2005; Bontognali *et al.* 2010). For example,

Arp *et al.* (2003) noted some biofilm laminae in subfossil microstromatolites from a marine-influenced crater lake in Indonesia had undergone replacement by Mg–Si. Bontognali *et al.* (2010) identified the potential for Mg and silica to be concentrated in EPS in microbial mats in recent microbial mats from Abu Dhabi. Burne *et al.* (2014) recorded Mg-silicates (stevensite) in modern thrombolites from Lake Clifton in Western Australia, which provides the structural rigidity for thrombolite growth, produced by biofilm mineralization, with aragonite growing in the stevensite matrix. In a more ancient example, Tosca *et al.* (2011) have explained the association of microbialites and early talc in Neoproterozoic carbonates as potentially reflecting microbial activity in influencing porewater chemistry. Wright & Barnett (2015) have identified multi-metre-scale cyclothems in the Barra Velha Formation of the Santos Basin, offshore Brazil, in which stevensite was a common matrix, but direct evidence for a microbial influence is certainly absent from the associated carbonates: these authors invoked evaporation as the likely trigger for large-scale stevensite precipitation.

Sedimentological implications of Mg-silicate nucleation and gel formation

Once the nucleation boundary is crossed, nucleation of Mg-silicates from water does not immediately produce a crystalline clay mineral but, instead, produces a Mg-silicate 'gel'. This precipitation pathway undoubtedly influences early and later diagenetic reactions and sedimentary textures in many non-marine carbonates.

There is abundant experimental and field-based evidence to support this pathway. For example, in their experimental study of Mg-silicate (including stevensite) precipitation from water at 25°C, Tosca & Masterson (2014) showed that the initial stages of stevensite precipitation occur rapidly (e.g. minutes to hours) upon crossing the critical supersaturation, producing a 'gel-phase' characterized by stevensite crystallites that exhibit limited stacking order and a high degree of hydration (e.g. between 20 and 30 wt% H_2O). The 'gel' phase, then, is simply defined as a hydrated aggregate of Mg-silicate nanoparticles, and is evidently persistent through the early diagenetic stages of lacustrine and peri-marine sediments. For example, a number of authors have reported the observation of Mg-silicate 'gels', 'poorly developed clays' or 'poorly crystalline silicates' (Millot 1970; Jeans 1971; Brindley *et al.* 1977; Gac *et al.* 1977; Calvo *et al.* 1999; Pozo & Casas 1999; Leveille *et al.* 2000, 2002; Polyak & Guven 2000; De Santiago Buey *et al.* 2000; Miller & James 2012). The environments in which these gel phases are most often found commonly involve fluids at high solute concentration (i.e. strongly supersaturated with respect to Mg-silicates), high salinity and pH, and most often include speleothems, evaporitic lacustrine environments and saline porewater. The results reported in these studies are in general agreement with those of Tosca & Masterson (2014) in terms of structural aspects detectable from X-ray diffraction (XRD), Fourier transform infrared spectroscopy (FT-IR) and thermal analysis. Indeed, the precipitation of a hydrated 'poorly crystalline' precursor appears to be a common pathway involved in the *de novo* formation of Mg-silicates from supersaturated solutions, thereby providing a link between experimental results and numerous occurrences of Mg-silicate 'gel'. In fact, because of the viscous nature of the gel and because of its role in removing Mg^{2+} from water (especially if the Mg/Si ratio in the fluid is less than that of stevensite), Wright (2012) suggested that stevensite gel might act as an ideal substrate for spherulitic calcite precipitation, which would explain some of the unusual textures observed in Santos Basin carbonates. Because the gel phase has been reported in lacustrine and peri-marine subsurface sediments in addition to those exposed to overlying bottom water (e.g. Pozo & Casas 1999; De Santiago Buey *et al.* 2000; Leveille *et al.* 2000, 2002; Polyak & Guven 2000; Miller & James 2012), the gel phase evidently persists in the subsurface, with the kinetics of dehydration dependent on the factors discussed above. Thus, Mg-silicate gels provide an important source of late diagenetic water to buried sediment, as well as a unique chemical and physical substrate to mediate further diagenetic reactions upon burial.

This Mg-silicate precipitation pathway predicts that a number of diagenetic reactions will take place between the initially precipitated gel and the surrounding sediments. For example, dehydration will ultimately take place upon the deposition of Mg-silicate gel, and this may occur in response to wetting–drying cycles, prolonged exposure to high-salinity solutions (i.e. low a_{H_2O}) or upon even shallow burial and mild heating (as most H_2O is released at very low temperatures during thermal analysis: see Tosca & Masterson 2014). Indeed, 'gel-dehydration' has been invoked by a number of authors as an important driver to explain the development of Mg-silicate minerals in evaporative environments and during sediment diagenesis (Gac *et al.* 1977; Stoessell & Hay 1978; Darragi & Tardy 1987; Pozo & Casas 1999). Gel dehydration was invoked as a main driver for the formation of kerolite associated with microbial mats in speleothems in basaltic caves found in Hawaii (Leveille *et al.* 2000, 2002). A similar dehydration pathway was suggested to explain stevensite associated

with evaporitic deposits from saline lakes (Gac *et al.* 1977; Stoessell & Hay 1978; Darragi & Tardy 1987; Pozo & Casas 1999; De Santiago Buey *et al.* 2000). Indeed, gel dehydration has also been implicated in explaining sedimentary textures associated with palygorskite- and sepiolite-bearing ooids formed in palustrine settings influenced by wetting–drying cycles (Miller & James 2012). The common feature of all of these environments involves initially high supersaturation states with respect to Mg-silicate minerals and environments driving the prolonged and, perhaps, cyclic dehydration of initially formed products. Importantly, because the initial gel phase may incorporate between 20 and 30 wt% H_2O even after drying at room temperature (Tosca & Masterson 2014), this may represent an important basinal fluid source to drive the destabilization of other minerals upon burial.

The sedimentological aspects of gel formation require additional consideration. Such gels are likely to accumulate in specific low-energy settings and where they will not be exposed to desiccation. They are unlikely to accumulate around lake margins where exposure and wave reworking will occur, so should be more characteristic of deeper sublittoral areas, although, as discussed below, not necessarily in organic-rich profundal settings. In small lakes or ponds with limited fetch, Mg-silicate gels have the potential to accumulate in relatively shallow settings, although the gels would then be prone to exposure.

Early diagenesis, Mg-silicate dissolution and porosity formation

Once Mg-silicates are deposited, there are a number of factors that can lead to their destabilization and subsequent dissolution during diagenesis. However, evidence of Mg-silicate (e.g. stevensite) dissolution, as documented from field settings, and the underlying reasons for this rather unusual phenomenon have not received much attention in the literature. From first principles, a simple shift in the saturation state of a given porewater with respect to Mg-silicates will establish a thermodynamic drive towards dissolution. Once this drive is established, dissolution and removal will take place at rapidly, controlled in part by the structure and bonding characteristics discussed above, and also by the extremely high specific surface area inherent to Mg-silicates. Under what conditions would such a drive for dissolution be established? Once this happens, how long would Mg-silicates persist in lacustrine sediments, and would this process affect surrounding carbonate sediments?

Lake Turkana, a brackish Na–HCO_3 lake of the East African rift system, offers important insight into how a thermodynamic drive for Mg-silicate dissolution could be established and also how labile Mg-silicate phases can be under certain chemical conditions. Stevensite is an important early precipitate from the lake water at Turkana, as demonstrated by cation mass balance and mineralogical analyses (Cerling 1979, 1996; Yuretich & Cerling 1983). Stevensite forms directly from evaporating lake water, which in turn exerts a strong control on Mg^{2+} depletion of the overall basin (Yuretich & Cerling 1983; Cerling 1996). In a detailed study of porewater chemistry at Lake Turkana, Cerling (1996) found that a number of sediment cores showed chemical variations with depth, indicating a diagenetic process not previously identified in lacustrine sediments. Specifically, Cerling (1996) observed increases in excess alkalinity with depth (mostly dominated by carbonate alkalinity), and further showed that these alkalinity increases were accompanied by releases in both Mg^{2+} and $SiO_{2(aq)}$ corresponding to a Mg/Si ratio stoichiometrically equivalent to stevensite. Because dissolved SO_4 is depleted in the Turkana porewaters and the $\delta^{13}C$ composition of the dissolved inorganic carbon (DIC) from these waters progressively increases with depth, Cerling (1996) argued that methanogenesis (only efficient in the near-absence of dissolved sulphate: Hoehler *et al.* 2010) triggered these changes. Methanogenesis, or the microbial generation of methane, typically occurs via one of two possible pathways (Canfield *et al.* 2005): (1) the reduction of CO_2 by H_2; or (2) the fermentation of organic matter, specifically acetate or other organic substrates, to produce methane and dissolved inorganic carbon. The second pathway is typically more important in non-marine sediments (Canfield *et al.* 2005) and results in CH_4 that is highly enriched in ^{12}C, and DIC that is highly enriched in ^{13}C. In addition to down-core increases in carbonate alkalinity (from organic matter fermentation), Mg^{2+} and $SiO_{2(aq)}$, Cerling (1996) also observed a significant increase in the $\delta^{13}C$ of DIC, supporting the idea that methanogenesis drove stevensite dissolution in lake Turkana sediments with depth.

The latter observation suggests that the carbon isotope composition of lacustrine carbonates may, in fact, be a useful guide in identifying processes that may have influenced the alkalinity budget of sediments during early diagenesis, perhaps initiating the corrosion of Mg-silicates (e.g. methanogenesis). However, the $\delta^{13}C$ composition of lacustrine carbonates may be influenced by a number of factors, including the composition of input waters, atmospheric CO_2 exchange and the mixing of gas sources produced by microbial respiration (e.g. Gierlowski-Kordesch 2010). Particularly relevant to Mg-silicate-rich systems, however, are changes in the relative amounts of authigenic dolomite and

calcite, which may be driven by changes in Ca and Mg availability (among many other factors). This may in turn affect the bulk $\delta^{13}C$ composition because the mineral-specific fractionation factors for dolomite and calcite are offset from one another (e.g. Bristow *et al.* 2012). These caveats indicate that an integrated mineralogical, geochemical and isotopic approach is needed to establish reliable fingerprints of early diagenetic Mg-silicate corrosion. Nevertheless, the basic observation from Lake Turkana that a silicate mineral such as stevensite shows rapid dissolution behaviour in preference to calcium carbonate sediments is, at first glance, a rather unusual one: it raises the broader question of why such a phenomenon might occur in lacustrine sediments and whether it might be a more general process to which Mg-silicates are particularly susceptible.

To illustrate why stevensite dissolution should occur in the Lake Turkana sediments, we have constructed a simple thermodynamic model exploring how porewater chemistry is modified by methanogenesis. Here, we use a thermodynamic model detailed in Tosca & Masterson (2014) that uses the Pitzer ion interaction model for calculating ion activity coefficients and, therefore, mineral saturation states in high ionic strength waters.

As a starting point, our calculations begin with the initial chemical composition of Lake Turkana water, as reported in Cerling (1996). Here the water has a pH of approximately 9.2 and is initially supersaturated with respect to stevensite, despite being somewhat depleted in Mg^{2+} (from widespread stevensite formation, as discussed above). The most important chemical change occurring in response to methanogenesis is the addition of excess DIC from the fermentation of organic substrates. These changes can be very simply modelled by adding dissolved inorganic carbon to the system as HCO_3^-. In the model, this is also equivalent to adding CO_2 in dissolved form (Fig. 3a) because, regardless of the form of DIC added to the water (e.g. $CO_{2(aq)}$, HCO_3^- or CO_3^{2-}), the distribution of carbonate species is dictated by both the equilibrium thermodynamics and the prevailing pH of the lake Turkana system.

As HCO_3^- is added to the Lake Turkana water, the increase in carbonate alkalinity rapidly shifts the pH from 9.2 to approximately 8.5 as about 60 mmol/kg HCO_3^- is added. At this endpoint in our calculations, the pH and alkalinity values of the simulated porewater are nearly identical to those compositions reported in Cerling (1996). This simple change has marked effects on the saturation state of Mg-silicate minerals. Because Mg-silicate phases display a thermodynamic and kinetic sensitivity to pH, the decrease from pH 9.2 to 8.5 causes stevensite to shift from supersaturated (in the initial Lake Turkana water) to undersaturated (in the porewater once methanogenesis is established) (Fig. 3b). At the same time, because porewater chemistry is effectively buffered by the carbonate system, the saturation states with respect to carbonate minerals actually show slight increases in saturation state and, therefore, remain unsusceptible to dissolution. This provides convincing evidence that small changes in carbonate alkalinity, driven, for example, by the microbial diagenesis

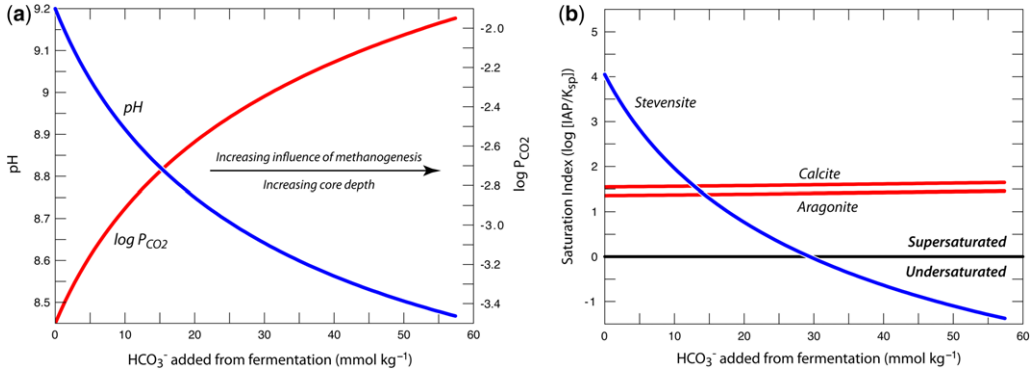

Fig. 3. Thermodynamic model calculations illustrating the effect of methanogenesis on Lake Turkana porewater chemistry. **(a)** Evolution of porewater pH (left axis) and dissolved CO_2 (right axis) during methanogenesis. As methanogenesis produces dissolved inorganic carbon (DIC), the pH of the original water (corresponding to Lake Turkana water reported in Cerling 1996) decreases from 9.2 to less than 8.5, closely corresponding to the porewater chemistry reported by Cerling (1996). **(b)** Calculated saturation states of stevensite, calcite and aragonite during methanogenesis in Lake Turkana porewater. The resulting pH decreases and DIC increases result in negligible effects on carbonate mineral stability, but result in porewaters that are undersaturated with respect to stevensite, enabling dissolution to proceed. IAP, ion activity product; K_{sp}, solubility product.

of organic matter, are effective in pushing Mg-silicates outside of their thermodynamic stability windows, establishing a thermodynamic drive for dissolution.

At first glance, it is somewhat unexpected that the pH values associated with stevensite dissolution in the Lake Turkana cores reach a minimum of around 8.5, yet are able to dissolve stevensite. This indicates that acidic conditions are not necessarily required to dissolve stevensite, so long as thermodynamic undersaturation is established. A related question, however, is why stevensite appears to dissolve so rapidly in the Lake Turkana cores once this undersaturation is established. We can understand this better by returning to the effects of the stevensite crystal structure and particle size on dissolution rate and the lifetime of stevensite in undersaturated sediment porewater.

Aside from the bonding types and crystal structure of stevensite as outlined above, one additional factor causing rapid dissolution lies in its high specific surface area. Like most clay minerals that form under Earth surface conditions, stevensite occurs in a variety of morphological crystal forms that are, at a maximum, of the order of hundreds of nanometres in size (Wilson 2013). In fact, neoformed stevensite has been shown to occur as distinctive spheres ranging from 50 to 1000 Å in diameter (or 100 nm maximum: De Santiago Buey *et al.* 2000; Benhammou *et al.* 2009). As a consequence, the specific surface area of stevensite has been reported to lie between 150 and 400 $m^2 g^{-1}$, roughly equivalent to the area of a tennis court contained in 1 g. Freshly precipitated stevensite, expected upon initial precipitation from evaporating lake water, undoubtedly lies at the upper end of this range and, perhaps, beyond. Regardless of exact values, the very small size of discrete stevensite particles means that in the presence of a thermodynamic drive for dissolution, the lifetime of these particles within a sediment might be expected to be far lower than many other minerals. This can be quantitatively illustrated if we assume a dissolution rate for stevensite using laboratory dissolution rates measured for crystalline talc as a structural analogue (Saldi *et al.* 2007). If we assume far-from-equilibrium dissolution rates for talc at pH 8.5 (from Saldi *et al.* 2007) and a discrete spherical particle size of 100 nm (e.g. De Santiago Buey *et al.* 2000), then by using the molar volume of stevensite and a simple kinetic relationship between dissolution rate and mineral lifetime (Lasaga 1998), we estimate that, under the Lake Turkana porewater conditions, individual stevensite particles would last no longer than about 70 years. Although there are large uncertainties inherent in this calculation, this is broadly consistent with the indications of rapid stevensite dissolution from the Lake Turkana cores (Cerling 1996), and also with reports of near-instantaneous removal of Mg-silicate scale at circum-neutral pH (e.g. Gunnlaugsson & Einarsson 1989). Indeed, these calculations show that, once a thermodynamic undersaturation for stevensite exists, complete dissolution occurs in a geological instant.

Mg-silicates may also be prone to destabilization during later diagenetic reactions initiated upon burial. For example, the thermal energy supplied upon burial often leads to the migration of cations from interlayer (exchangeable) positions to vacant octahedral sites (Jaynes & Bigham 1987; Jaynes *et al.* 1992; Komadel *et al.* 2005; Petit *et al.* 2008). This process, known as the Hofmann–Klemen effect, occurs mainly in montmorillonite-group clay minerals, to which stevensite belongs. Stevensite itself would be particularly vulnerable to this process because its structure demands that at least 10% of octahedral sites are vacant (Faust & Murata 1953). Univalent cations (e.g. Na^+ and Li^+) are most susceptible to migration in the stevensite structure, and divalent cations may also migrate (Jaynes & Bigham 1987; Jaynes *et al.* 1992; Komadel *et al.* 2005; Petit *et al.* 2008). Importantly, the migration of cations within the structure produces a loss of layer charge and expandability, and the generation of 'talc-like' species. Along with these changes, the loss of a proton from structural hydroxyl (-OH) groups occurs (Jaynes *et al.* 1992; Komadel *et al.* 2005; Petit *et al.* 2008), which would produce acidic porewater. In this way, stevensite may initiate its own self-destruction and dissolution resulting from cation migration driven by shallow burial.

Discussion and summary

Based on the considerations above, Mg-silicates formed in lacustrine settings should display a series of what might be termed 'behaviours' that can help in understanding and predicting their distribution and subsequent diagenesis. In terms of distribution, they not only require highly alkaline conditions, commonly met by the carbonate alkalinity provided in rifts with high volcanic activity, but also a specific chemistry. As discussed above, this chemistry may be generated through a number of means, but the most rapid and laterally extensive mechanism is through evaporative concentration. In the case of the Barra Velha Formation of Brazil, the abundance of calcite and Mg-silicates and the absence of the more typical evaporite minerals such as chlorides and sulphates, supports the view that the catchment areas were draining basic volcanic terrains. Wright (2012) also highlighted these controls, following the proposal from Cerling (1994) that lakes where volcanic terrains predominate tend to produce calcite,

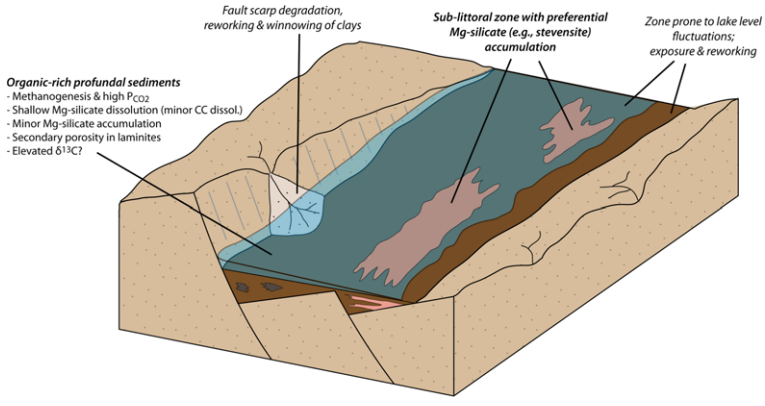

Fig. 4. Modelled distribution of Mg-silicates in an idealized rift-basin setting. Shallower but sub-littoral waters prone to evaporative concentration commonly cross the supersaturation boundary required for nucleation directly from water, and are less prone to the reworking and exposure that results in the largest and most widespread accumulations. Sediments deposited in deeper profundal settings are strongly influenced by organic matter diagenesis. Here methanogenesis, for example, would result in higher DIC (and dissolved CO_2 partial pressure (P_{CO_2})) conditions, where Mg-silicates would commonly destabilize and dissolve, imparting heavy $\delta^{13}C$ compositions to DIC that may be transferred to the carbonate sediments. CC, calcite.

tri-octahedral smectite, analcime and various bicarbonate–carbonate minerals. What remains unclear is whether a sufficient source of both Mg and $SiO_{2(aq)}$ was available to fuel the extensive precipitation of Mg-silicates in these Cretaceous lakes. An unusual and alternative source of solutes might be from the serpentinization of the mantle. Zalan *et al.* (2011) have shown that the Santos, Campos and Espírito Santo basins are all expressions of a magma-poor passive margin, and argue for the presence of a continuous belt of exhumed mantle at the transition between continental and oceanic crusts that flanks all three basins. They infer that serpentinization of exhumed mantle, deduced from gravimetric modelling, occurred down to depths of 6–8 km. This suggestion notwithstanding, direct evidence of serpentinization and/or the presence of exhumed mantle in the offshore Brazilian basins has remained elusive.

In summary, given suitable geochemical conditions, Mg-silicate gels are predicted to accumulate in lower-energy settings below wave base, and not prone to exposure, desiccation and reworking (Fig. 4). However, the effects of methanogenesis in profundal areas where organic matter could be concentrated implies that Mg-silicates would be more prone to destabilization and dissolution, so reducing the likelihood of accumulations in such settings. Although methanogenesis is demonstrably effective in tipping the porewater alkalinity balance in favour of Mg-silicate dissolution and carbonate precipitation, any process that disrupts this balance (i.e. decreases pH and Mg-silicate saturation, but increases carbonate alkalinity) will produce the same effect. Thus, from a facies model standpoint, we are left with a 'Goldilocks' situation where Mg-silicates would not accumulate in sediments deposited in waters that were too shallow or potentially too deep. Shallow closed-system lakes are, in reality, characteristically dynamic and so the actual distribution of Mg-silicates is expected to exhibit more complexity, with controls on chemistry and also with accommodation space playing a critical role. In rift settings, the updip regions of

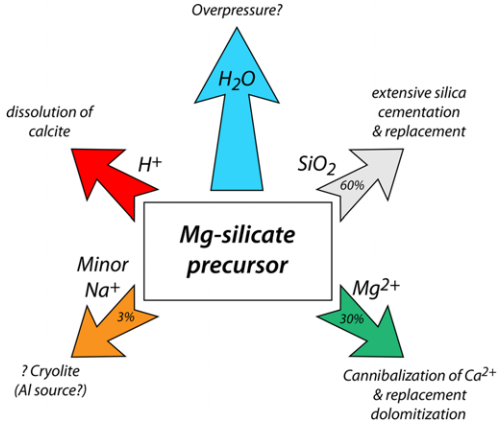

Fig. 5. Schematic showing the relative proportions of chemical components released from stevensite dissolution, and their primary diagenetic products.

half-graben are prone both to differential tilting and to footwall uplift, and so these might be seen as poor sites for Mg-silicate gel accumulation. Deeper settings (e.g. in lows adjacent to main faults), however, are expected to result in the highest levels of organic matter accumulation in profundal zones, promoting, for example, methanogenesis (Fig. 4) (Bosence 1998).

The congruent dissolution of Mg-silicates, leaving no direct *in situ* product, is likely to produce porosity. Wright & Barnett (2015) have identified petrographical criteria for identifying porosity formed after the dissolution of stevensite in the Barra Velha Formation of the Santos Basin. One of the most distinctive manifestations of this effect is seen in the widespread pseudo-fenestral porosity seen in the spherulitic facies. The resulting pore systems are illustrated by Terra *et al.* (2010) (their figs 20 & 21, especially fig. 20b).

Complete decay of the Mg-silicates would result in the release of Mg (30%), silica (60%) and minor Na (3%), in addition to bound water (Fig. 5). Thus, expected diagenetic products would include replacement dolomites (as the Mg^{2+} cannibalized any existing calcite), extensive silica cementation and replacement, and Na-silicates. The release of bound water might contribute to local overpressure, which would limit physical and chemical compaction. These products all fit with anecdotal evidence that the Barra Velha shows replacement dolomitization, extensive silicification, the presence of cryolite (although the source of Al is unresolved), and the survival of open-packed pore systems and the rarity of stylolites.

Jones & Xiao (2013) have proposed that geothermal convection linked to localized conduits might also be a critical factor in enhancing porosity and permeability in lacustrine carbonates sealed by salt, as in the specific case of the Barra Velha Formation in the Santos Basin. The study implies an awareness that late-stage corrosion has affected these carbonates (as is also our experience), but an alternative process that could cause later-stage dissolution could also reflect an inherent property of the decay on Mg-silicates, specifically the production of protons by the Hofmann–Klemen effect, discussed earlier. If this operated in the Barra Velha Formation, it would produce a more widespread dissolution effect and not one linked to major fluid conduits such as faults – a testable alternative model if and when more data become available from the region.

In summary, although both the occurrence and diagenetic consequences of Mg-silicates in carbonate reservoirs are somewhat unfamiliar from the standpoint of petroleum geology, many enigmatic features can be understood from first-principle considerations rooted in geochemistry, mineralogy and sedimentology. The model presented here provides a novel framework for understanding and predicting Mg-silicate–carbonate interactions and their geological consequences, and should provide a fertile starting point to develop and test new hypotheses for porosity evolution as data continue to emerge.

The authors thank Andrew Barnett, Frances Abbotts, and Rachel Wood for helpful discussion, and Jeff Lukasik and an anonymous reviewer for thoughtful reviews.

References

Arp, G., Reimer, A. & Reitner, J. 2003. Microbialite formation in seawater of increased alkalinity, Satonda Crater Lake, Indonesia. *Journal of Sedimentary Research*, **73**, 105–127.

Bailey, S. W. 1980. Structures of layer silicates. *In*: Brindley, G. W. & Brown, G. (eds) *Crystal Structures of Clay Minerals and their X-ray Diffraction*. Mineralogical Society, London, 1–124.

Barbiéro, L., de Queiroz Neto, J. P., Ciornei, G., Sakamoto, A. Y., Capellari, B., Fernandes, E. & Valles, V. 2002. Geochemistry of water and ground water in the Nhecolândia, Pantanal of Mato Grosso, Brazil: variability and associated processes. *Wetlands*, **22**, 528–540.

Benhammou, A., Tanouti, B., Nibou, L., Yaacoubi, A. & Bonnet, J.-P. 2009. Mineralogical and physicochemical investigation of Mg-smectite from Jbel Ghassoul, Morocco. *Clays and Clay Minerals*, **57**, 264–270.

Bontognali, T. R. R., Vasconcelos, C., Warthmann, R. J., Bernasconi, S. M., Dupraz, C., Strohmenger, C. J. & McKenzie, J. A. 2010. Dolomite formation within microbial mats in the coastal sabkha of Abu Dhabi (United Arab Emirates). *Sedimentology*, **57**, 824–844.

Bosence, D. W. J. 1998. Stratigraphic and sedimentological models of rift basins. *In*: Purser, B. H. & Bosence, D. W. J. (eds) *Sedimentation and Tectonics of Rift Basins: Red Sea–Gulf of Aden*. Chapman & Hall, London, 9–25.

Brantley, S. L. 2008. Kinetics of mineral dissolution. *In*: Brantley, S. L., Kubicki, J. & White, A. F. (eds) *Kinetics of Water–Rock Interaction*. Springer, Berlin, 151–210.

Brindley, G. W., Bish, D. L. & Wan, H. M. 1977. Nature of kerolite and its relation to talc and stevensite. *Mineralogical Magazine*, **41**, 443–452.

Bristow, T. F., Kennedy, M. J., Morrison, K. D. & Mrofka, D. D. 2012. The influence of authigenic clay formation on the mineralogy and stable isotopic record of lacustrine carbonates. *Geochimica et Cosmochimica Acta*, **90**, 64–82.

Burne, R. V., Moore, L. S., Christy, A. G., Troitzsch, U., King, P. L., Carnerup, A. M. & Hamilton, P. J. 2014. Stevensite in the modern thrombolites of Lake Clifton, Western Australia: a missing link in microbialite mineralization? *Geology*, **42**, 575–578, https://doi.org/10.1130/G35484.1

Calvo, J. P., Blanc-Valleron, M. M., Rodriguez-Arandia, J. P., Rouchy, J. M. & Sanz, M. E. 1999. Authigenic clay minerals in continental evaporitic environments. *In*: Thiry, M. & Simon-Coinçon, R. (eds) *Palaeoweathering, Palaeosurfaces and Related Continental Deposits*. International Association of Sedimentologists, Special Publications, **27**, 129–151.

Canfield, D. E., Kristensen, E. & Thamdrup, B. 2005. *Aquatic Geomicrobiology*. Elsevier, Amsterdam.

Casey, W. H. & Ludwig, C. 1995. Silicate mineral dissolution as a ligand exchange reaction. *In*: White, A. F., Brantley, S. L. & Ribbe, P. H. (eds) *Chemical Weathering Rates of Silicate Minerals*. Reviews in Mineralogy and Geochemistry, **31**. Mineralogical Society of America, Washington, DC, 87–118.

Casey, W. H. & Westrich, H. R. 1992. Control of dissolution rates of orthosilicate minerals by divalent metal-oxygen bonds. *Nature*, **355**, 157–159.

Cerling, T. E. 1979. Paleochemistry of plio-pleistocene lake Turkana, Kenya. *Palaeogeography, Palaeoclimatology, Palaeoecology*, **27**, 247–285.

Cerling, T. E. 1994. Chemistry of closed basin lake waters: a comparison between African Rift Valley and some central North American rivers and lakes. *In*: Gierlowski-Kordesch, E. H. & Kelts, K. (eds) *The Global Geological Record of Lake Basins*, **1**. Cambridge University Press, Cambridge, 29–30.

Cerling, T. E. 1996. Pore water chemistry of an alkaline lake: Lake Turkana, Kenya. *In*: Johnson, T. C. & Odada, E. O. (eds) *Limnology, Climatology and Paleoclimatology of the East African Lakes*. Gordon and Breach, Amsterdam, 225–240.

Darragi, F. & Tardy, Y. 1987. Authigenic trioctahedral smectites controlling pH, alkalinity, silica and magnesium concentrations in alkaline lakes. *Chemical Geology*, **63**, 59–72.

Deocampo, D. M., Cuadros, J., Wing-Dudek, T., Olives, J. & Amouric, M. 2009. Saline lake diagenesis as revealed by coupled mineralogy and geochemistry of multiple ultrafine clay phases: Pliocene Olduvai Gorge, Tanzania. *American Journal of Science*, **309**, 834–858.

De Santiago Buey, C., Barrios, M. S., Romero, E. G. & Montoya, M. D. 2000. tMg-rich smectite 'precursor' tphase in the Tagus basin, Spain. *Clays and Clay Minerals*, **48**, 366.

Drits, V. A., Guggenheim, S., Zviagina, B. B. & Kogure, T. 2012. Structures of the 2:1 layers of pyrophyllite and talc. *Clays and Clay Minerals*, **60**, 574–587.

Eugster, H. P. & Jones, B. F. 1979. Behavior of major solutes during closed-basin brine evolution. *American Journal of Science*, **279**, 609–631.

Evans, B. W. & Guggenheim, S. 1988. Talc, pyrophyllite, and related minerals. *In*: Bailey, S. W. (ed.) *Hydrous Phyllosilicates*. Reviews in Mineralogy, **19**. Mineralogical Society of America, Washington, DC, 225–294.

Faust, G. T. & Murata, K. J. 1953. Stevensite, redefined as a member of the montmorillonite group. *American Mineralogist*, **38**, 973–987.

Faust, G. T., Hathaway, J. C. & Millot, G. 1959. A restudy of stevensite and allied minerals. *American Mineralogist*, **44**, 342–370.

Gac, J. Y., Droubi, A., Fritz, B., & Tardy, Y. 1977. Geochemical behaviour of silica and magnesium during the evaporation of waters in Chad. *Chemical geology*, **19**, 215–228.

Galán, E. & Pozo, M. 2011. Palygorskite and sepiolite deposits in continental environments. Description, genetic patterns and sedimentary settings. *In*: Galan, E. & Singer, A. (eds) *Developments in Palygorskite–Sepiolite Research*. Developments in Clay Science, **3**. Elsevier, Amsterdam, 125–173.

Gierlowski-Kordesch, E. H. 2010. Lacustrine carbonates. *In*: Alonso-Zarza, A. M. & Tanner, E. H. (eds) *Carbonates in Continental Settings: Facies, Environments and Processes*. Developments in Sedimentology, **61**. Elsevier, Amsterdam, 1–101.

Guggenheim, S. & Eggleton, R. A. 1987. Modulated 2: 1 layer silicates; review, systematics, and predictions. *American Mineralogist*, **72**, 724–738.

Guggenheim, S. & Krekeler, M. P. 2011. The structures and microtextures of the palygorskite–sepiolite group minerals. *In*: Galan, E. & Singer, A. (eds) *Developments in Palygorskite–Sepiolite Research. A New Outlook on these Nanomaterials*. Developments in Clay Science, **3**. Elsevier, Amsterdam, 1–32.

Gunnlaugsson, E. & Einarsson, A. R. 1989. Magnesium-silicate scaling in mixture of geothermal water and deaerated fresh water in a district heating system. *Geothermics*, **18**, 113–120.

Hoehler, T., Gunsalus, R. P. & McInerney, M. J. 2010. Environmental constraints that limit methanogenesis. *In*: Timmis, K. N. (ed.) *Handbook of Hydrocarbon and Lipid Microbiology*. Springer, Berlin, 636–654.

Jaynes, W. F. & Bigham, J. M. 1987. Charge reduction, octahedral charge, and lithium retention in heated, Li-saturated smectites. *Clays and Clay Minerals*, **35**, 440–448.

Jaynes, W. F., Traina, S. J., Bigham, J. M. & Johnston, C. T. 1992. Preparation and characterization of reduced-charge hectorites. *Clays and Clay Minerals*, **40**, 397–404.

Jeans, C. V. 1971. The neoformation of clay minerals in brackish and marine environments. *Clays and Clay Minerals*, **9**, 209–217.

Jones, B. F. 1986. Clay mineral diagenesis in lacustrine sediments. *In*: Mumpton, F. A. (ed.) *Studies in Diagenesis*. United States Geological Survey, Bulletin, **1578**, 291–300.

Jones, B. F. & Bowser, C. J. 1978. The mineralogy and related chemistry of lake sediments. *In*: Lerman, A. (ed.) *Lakes: Chemistry, Geology and Physics*. Springer, Berlin, 179–227.

Jones, B. F. & Conko, K. M. 2011. Environmental influences on the occurrences of sepiolite and palygorskite: a brief review. *In*: Galan, E. & Singer, A. (eds) *Developments in Palygorskite–Sepiolite Research*. Developments in Clay Science, **3**. Elsevier, Amsterdam, 69–83.

Jones, B. F. & Galan, E. 1988. Sepiolite and Palygorskite. *In*: Bailey, S. W. (ed.) *Hydrous Phyllosilicates,* Reviews in Mineralogy, **19**. Mineralogical Society of America, Washington, DC, 631–674.

Jones, G. D. & Xiao, Y. 2013. Geothermal convection in South Atlantic subsalt lacustrine carbonates: developing diagenesis and reservoir quality predictive concepts with reactive transport models. *Bulletin American Association of Petroleum Geologists*, **97**, 1249–1271.

Komadel, P., Madejova, J. & Bujdak, J. 2005. Preparation and properties of reduced-charge smectites – a review. *Clays and Clay Minerals*, **53**, 313–334.

Lasaga, A. C. 1998. *Kinetic Theory in the Earth Sciences*. Princeton University Press, Princeton, NJ.

Leveille, R. J., Fyfe, W. S. & Longstaffe, F. J. 2000. Unusual secondary Ca-Mg-carbonate-kerolite deposits in basaltic caves, Kauai, Hawaii. *Journal of Geology*, **108**, 613–621.

Leveille, R. J., Longstaffe, F. J. & Fyfe, W. S. 2002. Kerolite in carbonate-rich speleothems and microbial deposits from basaltic caves, Kauai, Hawaii. *Clays and Clay Minerals*, **50**, 514–524.

Miller, A. K., Guggenheim, S. & Koster van Groos, A. F. 1991. Bond energy of adsorbed and interlayer water: kerolite dehydration at elevated pressures. *Clays and Clay Minerals*, **39**, 127–130.

Miller, C. R. & James, N. P. 2012. Autogenic microbial genesis of middle miocene palustrine ooids; Nullarbor Plain, Australia. *Journal of Sedimentary Research*, **82**, 633–647.

Millot, G. 1970. *Geology of Clays*. Springer, London.

Mitsuda, T. & Taguchi, H. 1977. Formation of magnesium-silicate hydrate and its crystallization to talc. *Cement and Concrete Research*, **7**, 223–230.

Noack, Y., Decarreau, A., Boudzoumou, F. & Trompette, R. 1989. Low-temperature oolitic talc in upper Proterozoic rocks, Congo. *Journal of Sedimentary Research*, **59**, 717.

Oelkers, E. H. 1999. A comparison of forsterite and enstatite dissolution rates and mechanisms. *In*: Jamtveit, B. & Meakin, P. (eds) *Growth, Dissolution and Pattern Formation in Geosystems*. Kluwer, Dordrecht, 253–268.

Oelkers, E. H. 2001*a*. An experimental study of forsterite dissolution rates as a function of temperature and aqueous Mg and Si concentrations. *Chemical Geology*, **175**, 485–494.

Oelkers, E. H. 2001*b*. General kinetic description of multioxide silicate mineral and glass dissolution. *Geochimica et Cosmochimica Acta*, **65**, 3703– 3719.

Oelkers, E. H. & Schott, J. 2001. An experimental study of enstatite dissolution rates as a function of pH, temperature, and aqueous Mg and Si concentration, and the mechanism of pyroxene/pyroxenoid dissolution. *Geochimica et Cosmochimica Acta*, **65**, 1219–1231.

Petit, S., Righi, D. & Decarreau, A. 2008. Transformation of synthetic Zn-stevensite to Zn-talc induced by the Hofmann-Klemen effect. *Clays and Clay Minerals*, **56**, 645–654.

Polyak, V. J. & Guven, N. 2000. Authigenesis of trioctahedral smectite in magnesium-rich carbonate speleothems in Carlsbad Cavern and other caves of the Guadalupe Mountains, New Mexico. *Clays and Clay Minerals*, **48**, 317.

Pozo, M. & Casas, J. 1999. Origin of kerolite and associated Mg clays in palustrine-lacustrine environments; the Esquivias Deposit (Neogene Madrid Basin, Spain). *Clay Minerals*, **34**, 395.

Renaut, R. W., Morley, C. K. & Jones, B. 2002. Fossil hot-spring travertine in the Turkana basin, northern Kenya: structure, facies, and genesis. *In*: Renaut, R. W. & Ashley, G. M. (eds) *Sedimentation in Continental Rifts*. Society for Sedimentary Geology (SEPM), Special Publications, **73**, 123–141.

Saldi, G. D., Köhler, S. J., Marty, N. & Oelkers, E. H. 2007. Dissolution rates of talc as a function of solution composition, pH and temperature. *Geochimica et Cosmochimica Acta*, **71**, 3446–3457.

Souza-Egipsy, V., Wierzchos, J., Ascaso, C. & Nealson, K. H. 2005. Mg-silica precipitation in fossilization mechanisms of sand tufa endolithic microbial community, Mono Lake (California). *Chemical Geology*, **217**, 77–87.

Stoessell, R. K. & Hay, R. L. 1978. Geochemical origin of sepiolite and kerolite at Amboseli, Kenya. *Contributions to Mineralogy and Petrology*, **65**, 255–267.

Stumm, W. 1992. *Chemistry of the Solid–Water Interface: Processes at the Mineral–Water and Particle–Water Interface in Natural Systems*. John Wiley, New York.

Terra, G. J. S., Spadini, A. R. *et al*. 2010. Classificação de rochas carbonáticas aplicável às bacias sedimentares [Carbonate rock classifcation applied to Brazilian sedimentary basins]. *Boletin Geociencias Petrobras*, **18**, 9–29.

Tosca, N. J. 2015. Geochemical pathways to Mg-clay formation. *In*: Pozo, M. & Galán, E. (eds) *Magnesian Clays: Characterization, Origins and Applications*. AIPEA (Association Internationale pour l'Etude des Argiles), Special Publications, **2**, 283–329.

Tosca, N. J. & Masterson, A. L. 2014. Chemical controls on incipient Mg-silicate crystallization at 25°C: implications for early and late diagenesis. *Clay Minerals*, **49**, 165–194.

Tosca, N. J., Macdonald, F. A., Strauss, J. V., Johnston, D. T. & Knoll, A. H. 2011. Sedimentary talc in Neoproterozoic carbonate successions. *Earth and Planetary Science Letters*, **306**, 11–22.

Wilson, M. J. 2013. *Rock-Forming Minerals, Volume 3C, Sheet Silicates: Clay Minerals*. Geological Society, London.

Wright, V. P. 2012. Lacustrine carbonates in rift settings: the interaction of volcanic and microbial processes on carbonate deposition. *In*: Garland, J., Neilson, J. E., Laubach, S. E. & Whidden, K. J. (eds) *Advances in Carbonate Exploration and Reservoir Analysis*. Geological Society, London, Special Publications, **370**, 39–47, https://doi.org/10.1144/SP370.2

Wright, V. P. & Barnett, A. 2015. An abiotic model for the development of textures in some South Atlantic early Cretaceous lacustrine carbonates. *In*: Bosence, D. W. J., Gibbons, K. A., Le Heron, D. P., Morgan, W. A., Pritchard, T. & Vining, B. A. (eds) *Microbial Carbonates in Space and Time: Implications for Global Exploration and Production*. Geological Society, London, Special Publications, **418**, 209–219, https://doi.org/10.1144/SP418.3

Yuretich, R. F. & Cerling, T. E. 1983. Hydrogeochemistry of Lake Turkana, Kenya: mass balance and

mineral reactions in an alkaline lake. *Geochimica et Cosmochimica Acta*, **47**, 1099–1109.

Zalan, P. V., do Carmo, M., Severino, G., Rigoti, C. A., Magnavita, L. P., Bach de Oliveira, J. A. & Vianna, A. R. 2011 An entirely new 3D-view of the crustal and mantle structure of a South Atlantic passive margin – Santos, Campos and Espírito Santo basins, Brazil. *American Association of Petroleum Geologists Annual Convention and Exhibition*, Houston, TX, USA, 10–13 April 2011, Search and Discovery Article #30177, http://www.searchanddiscovery.com/documents/2011/30177zalan/ndx_zalan.pdf